nature climate change

ARTICLES

https://doi.org/10.1038/s41558-018-0138-5

Anthropogenic warming exacerbates European soil moisture droughts

L. Samaniego[1,7*], S. Thober[1,7], R. Kumar[1], N. Wanders[2], O. Rakovec[1,3], M. Pan[4], M. Zink[1,6], J. Sheffield[5], E. F. Wood[4] and A. Marx[1]

Anthropogenic warming is anticipated to increase soil moisture drought in the future. However, projections are accompanied by large uncertainty due to varying estimates of future warming. Here, using an ensemble of hydrological and land-surface models, forced with bias-corrected downscaled general circulation model output, we estimate the impacts of 1–3 K global mean temperature increases on soil moisture droughts in Europe. Compared to the 1.5 K Paris target, an increase of 3 K—which represents current projected temperature change—is found to increase drought area by 40% (±24%), affecting up to 42% (±22%) more of the population. Furthermore, an event similar to the 2003 drought is shown to become twice as frequent; thus, due to their increased occurrence, events of this magnitude will no longer be classified as extreme. In the absence of effective mitigation, Europe will therefore face unprecedented increases in soil moisture drought, presenting new challenges for adaptation across the continent.

Global warming is projected to increase evaporation and to reduce soil moisture where it is present, at several hotspot locations around the globe[1,2]. Current research indicates that, although climate change may not create droughts, it may exacerbate them[3–8]. Consequently, droughts may set in more quickly, be more intense and last longer[9]. The recent Paris Agreement on climate change focuses on holding the global temperature increase to well below 2 K or even 1.5 K above pre-industrial levels[10]. It is worth noting that future global temperatures will probably exceed 2 K above pre-industrial levels by 2100[11]. Limiting global warming to these levels has unknown effects on the characteristics of soil moisture droughts (for example, drought area and duration) because these characteristics have been quantified for different future periods using emission scenarios that cover a wide range of temperature projections[9,12–15]. Moreover, the definition of a drought under a non-stationary climate must be carefully chosen such that drought events represent dry anomalies with respect to reference conditions[16]. The agricultural adaptation potential has been estimated for Europe, taking into account crop yield and profit per hectare[17]. Here, we quantify the extent and duration of future droughts and changes in aridity for different warming levels with and without adaptation (see Methods). We aim to provide information on the benefits of limiting global warming to 1.5 K relative to 3 K in terms of agricultural droughts, which have substantial impacts on vegetation stress, crop losses, the risk of forest fires, tourism[18], ecosystem services and GHG emissions[19].

The uncertainty in climate projections and hydrological model parameterizations introduces considerable variability into the resulting projections of the characteristics of soil moisture drought[20,21], thus highlighting the need for multimodel ensembles to enable comprehensive assessments of these events. However, studies of soil moisture droughts at continental and global scales are limited to a few ensemble members and/or employ a single hydrological model[22]. Existing multimodel analyses of future droughts focus primarily on hydrological droughts[13,21].

To address these shortcomings, we establish a modelling chain using multiple models to generate an unprecedentedly large (60-member) ensemble of high-resolution $5\times5\,km^2$ hydrological simulations that cover the European domain (see Methods). We use two hydrological models (HMs) and two land-surface models (LSMs) that employ a consistent set of land-surface properties. The two HMs use a temperature-based potential evapotranspiration (PET) scheme, which has been criticized within the application of drought analysis using the Palmer drought severity index (PDSI)[6,23]. The soil moisture index (SMI) derived from these HMs, however, does not show the same deficiency as the PDSI because of methodological differences in how these indices are estimated (see Methods). All HMs/LSMs are driven by downscaled forcings obtained from five bias-corrected Coupled Model Intercomparison Project Phase 5 (CMIP5) projections[24] that follow three representative concentration pathways (RCPs; RCP2.6, RCP6.0 and RCP8.5). To guarantee comparability across the multimodel ensemble, all HMs and LSMs estimate soil moisture up to a depth of 2 m and the estimated soil moisture values are transformed into a monthly SMI[20]. These high-resolution SMI fields are required to perform a spatio-temporal drought cluster analysis[20], which enables to quantify the area–duration characteristics of every soil moisture drought event. Based on this cluster analysis, two key drought characteristics—the area under drought and the drought duration—are estimated for all drought events simulated by each general circulation model (GCM) and HM/LSM model combination (see Methods). These two characteristics are then analysed for the largest drought within each GCM–HM/LSM combination over specific 30-year periods that correspond to different warming levels under the three RCPs[25]. A time sampling approach is used to extract future 30-year periods that correspond to global warming levels of 1.0, 1.5, 2.0, 2.5 and 3 K with respect to pre-industrial levels for each of the GCM/RCP projections[15] (see Methods). The period from 1971 to 2000 is selected to represent present-day conditions.

[1]UFZ-Helmholtz Centre for Environmental Research, Leipzig, Germany. [2]Physical Geography, Utrecht University, Utrecht, Netherlands. [3]Faculty of Environmental Sciences, Czech University of Life Sciences, Prague, Czech Republic. [4]Civil and Environmental Engineering, Princeton University, Princeton, NJ, USA. [5]Geography and Environment, University of Southampton, Southampton, UK. [6]Present address: European Centre for Medium-Range Weather Forecasts, Reading, UK. [7]These authors contributed equally: L. Samaniego and S. Thober. *e-mail: luis.samaniego@ufz.de

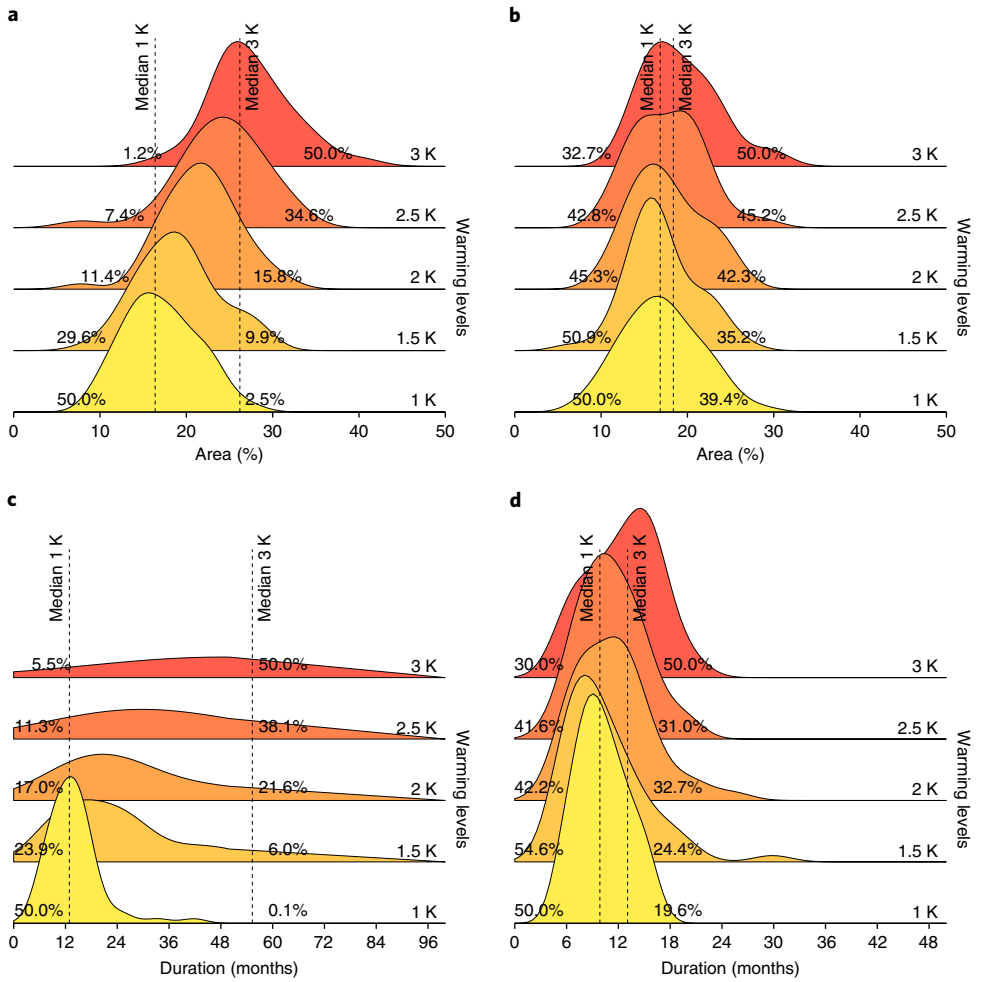

Fig. 1 | Distribution functions of drought areas and durations for different levels of global warming. a–d, Distribution functions are displayed for both the drought areas (**a**,**b**) and durations (**c**,**d**) of the largest drought events over the 30-year periods that correspond to each global warming level. The results are shown without adaptation (**a**,**c**) and with adaptation (**b**,**d**). The vertical dashed lines indicate the median values for global warming of 1 K and 3 K. The fractions of ensemble members located towards the tails are also denoted as percentages. The *x* axis limits are different for the durations with and without adaptation (**c**,**d**) for clarity.

Based on our multimodel ensemble analysis, Fig. 1a shows that the ensemble median of the largest drought area increases from 18.7% of the European territory under a warming of 1.5 K to 26.2% under a warming of 3 K. The drought threshold from the reference period 1971–2000 is used to enable comparison with historic events; that is, adaptation to climate change is not considered. If adaptation is not considered, then only the top 9.9% of simulated drought areas under a warming of 1.5 K exceed the ensemble median under a global warming of 3 K. Note that the percentage of ensemble members that exceeds the median of the 3 K ensemble increases nonlinearly with the degree of global warming. For example, this quantity increases by 13.3% (2.5% to 15.8%) as the amount of global warming increases from 1 K to 2 K; however, it increases by 34.2% as the amount of global warming increases from 2 K to 3 K.

Drought duration (Fig. 1c) also exhibits substantial changes across the different warming levels. The median duration of exceptional drought events shows approximately a two- to threefold increase between the 1.5 and 3 K warming levels (that is, it increases from 20 months under a warming of 1.5 K to approximately 55 months under a warming of 3 K). Given these changes in the distributions of the areas and the durations of extreme drought events, these future events may no longer represent droughts, which are defined as deviations from normal conditions. This analysis indicates that, for amounts of global warming equal to or greater than 1.5 K, the normal conditions that are used to define typical drought characteristics must be reassessed.

The impact of climate change on drought characteristics is strongly diminished after adaptation (meaning that the drought threshold is recalculated based on the projected soil moisture under different levels of global warming as indicated in the Methods) to climate change is considered. Overall, the ensemble median drought area is estimated to be between 16% and 18% of the European territory, and the duration is approximately 9 to 12 months for all of the considered warming levels. A significant difference is only found between the warming levels of 3 K and at most 1.5 K (applying a Kolmogorov–Smirnov test with a significance level of 5%, Fig. 1d). It is expected that drought area and duration would remain unchanged if the soil moisture drought threshold is estimated for each warming level separately (representing adaptation to climate change). Small deviations may still occur, however, because of the intrinsic uncertainty of the processes describing soil moisture dynamics. It is worth noting that these increases are also obtained using other SMI drought thresholds (see Methods, compare Fig. 1 and Supplementary Fig. 1).

The substantial increases in drought area and duration without adaptation (Fig. 1a,c) are not evenly distributed across the European

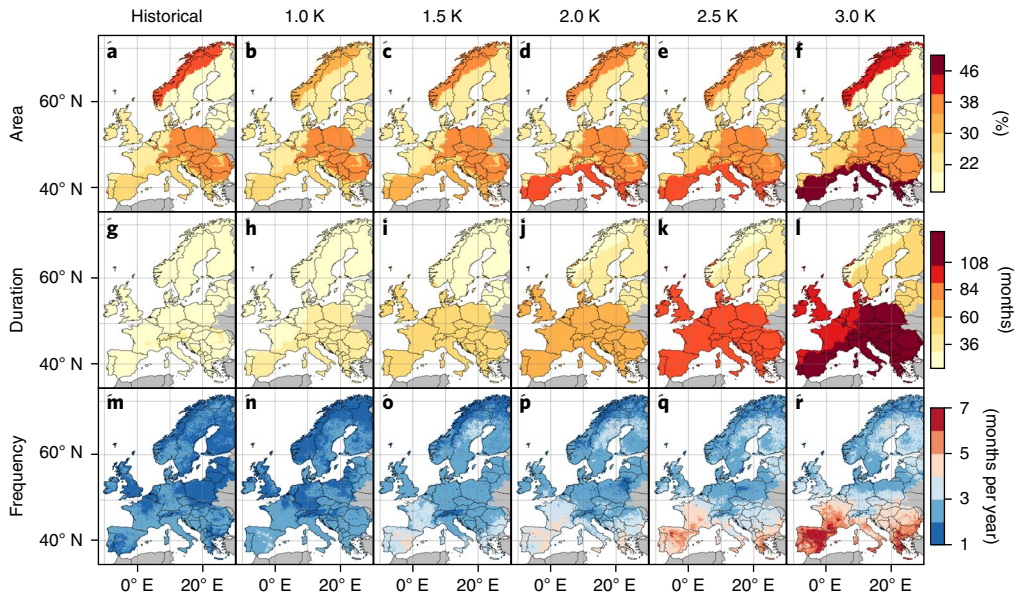

Fig. 2 | Spatial distribution of changes in drought area, duration and frequency. a–f, The area under drought is evaluated for the six IPCC AR5 regions[26] and quantified as a percentage of the total area of each region for the different levels of warming. **g–l**, The drought duration for the same regions and warming levels. The area under drought and the drought duration are both calculated for the multimodel median of the largest drought events. **m–r**, The frequency of drought months is depicted at the individual grid cell level, which is calculated from the multimodel median estimates. All of the results are calculated assuming no adaptation to climate change.

domain. Figure 2 depicts strong spatial differences in the drought area and duration over six major environmental regions in Europe (that is, the Alpine North, Atlantic, Boreal, Continental, Mediterranean and Alpine South regions; see Fig. 3a)[26,27]. The exact values are provided in Table 1. The largest increases in the drought area and duration are projected to occur in the Mediterranean. Compared with the estimates for the historical period (1971–2000), the drought area will change from 28% on average to 49% under a warming of 3 K (Fig. 2a,f). The increase in drought area is less than 10% in the Atlantic, Continental, Alpine North and Alpine South regions. Increased precipitation will decrease the drought area in the Boreal region by about 3% under a global warming of 3 K. Interestingly, the Alpine North region shows the highest percentage of drought area among all regions for the historic period 1971–2000 (Fig. 2a), which highlights that droughts have a higher spatial dependence in this region than in the other ones.

With the exception of the Alpine North and Boreal regions, the durations of the largest drought events are three to four times higher under a warming of 3 K compared to historical values (Table 1). The increases in drought duration are nonlinearly related to climate change because they double (at most) under a global warming of 2 K. The longest droughts, which have durations exceeding 10 years (120 months), are projected to occur in the Mediterranean, Alpine South and Continental regions under a global warming of 3 K. Overall, our results show an alteration of the hydrologic regimes in the Mediterranean and Continental regions when a warming level of 3 K is approached.

The frequency of drought events (expressed in terms of the number of drought months occurring per year) also exhibits marked regional and subregional differences, due mainly to the influence of local physiographic and climatic characteristics (Fig. 2m–r). During the historical period, the mean drought frequency for all of the grid cells in all of the regions is approximately 2 months per year. This historically low value increases to an unprecedentedly high value under climate change if no adaptation is considered. For example, the Mediterranean will experience a steady increase in this quantity as the warming level rises, reaching 5.6 months per year under 3 K. Note that some parts of the Iberian Peninsula are projected to experience more than seven drought months per year under the 3 K warming level (Fig. 2r). These events may no longer be considered droughts, given that they occur half of the time. All HMs project increases in drought frequency in the Mediterranean, which is a result of the reduced precipitation in this region (see Supplementary Figs. 2 and 3). The Continental region shows a change from 1–2 months per year to 3–5 months. Most locations in the Alpine South region will experience a shift in drought frequency from 1–2 months under present-day conditions to 4 months per year under a warming of 3 K.

The previous two figures highlight the need for constant adaptation to the changing climate and indicate that historic drought thresholds may not apply in the future. Adaptation of society to the new normal is known to be associated with substantial costs[28]. However, the crucial question for society as a whole, and water planners in particular, is what the new drought conditions that will occur under different warming levels imply for adaptation policies. To answer this fundamental question, the change in the drought threshold is estimated in a 2-m-deep soil column in litres per square metre (that is, in millimetres of soil water storage). This value is an indicator of the available soil water content under drought conditions and quantifies the change in aridity.

The resulting ensemble average change in the available soil water content is estimated over the six environmental regions for the different warming levels and seasons (winter, spring, summer and autumn), including their variability and statistical significance. The magnitude of this change generally increases with increased global warming and is significant for changes larger than 3% (Fig. 3). Two major patterns are observed: (1) the Mediterranean and Atlantic regions experience decreases in soil water content in all seasons and under all warming levels; and (2) the Alpine North, Alpine South, Boreal and Continental regions tend to become wetter in winter and spring and drier in summer and autumn.

The Mediterranean region is the most affected in all seasons (Fig. 3e), with the largest increase in aridity appearing in the winter and spring under all warming levels. At the 3 K warming level, the available soil water decreases by 35 mm (±24 mm), which

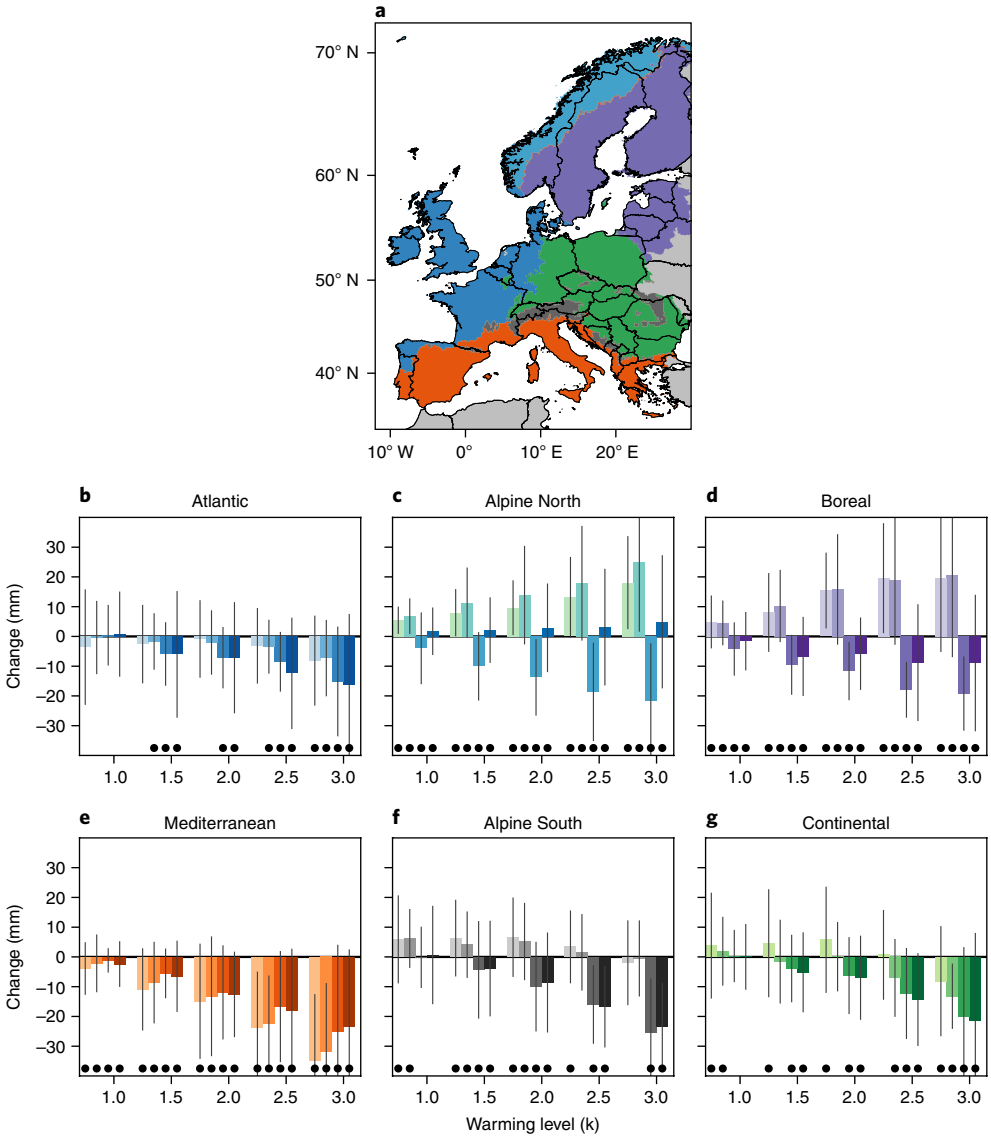

Fig. 3 | Changes in aridity for various warming levels. a, The IPCC AR5 regions[26]. **b**–**g**, Changes in the soil water availability (aridity) during drought events between a given warming level and the reference period, taking adaptation to climate change into account. The results are aggregated to the IPCC AR5 regions[26] for the different seasons (from left to right, DJF, MAM, JJA and SON) and for each warming level. The whiskers indicate the interquartile range of the multimodel ensemble results. The markers at the bottom of the plots indicate changes that differ significantly from zero, as determined using a Wilcoxon rank-sum test and a significance level of 5%.

corresponds to a shortage of 35,000 $m^3 km^{-2}$. The Atlantic region exhibits the smallest changes in the available soil water among all of the regions and for all of the warming levels (Fig. 3b). The Continental region exhibits positive changes during the winter for warming amounts of up to 2 K (Fig. 3g). In contrast, negative changes are observed for all of the warming levels above 1.5 K during the spring, summer and autumn. Earlier onsets of snowmelt cause increases in the available soil water in the winter and spring for all of the warming levels in the Alpine North and Boreal regions (Fig. 3c,d). These earlier onsets also lead to increases in aridity in these regions of up to 20 mm in summer, when snowmelt is no longer a source of water.

Global warming leads to significant intensification of European droughts, which confirms previous work[6]. We show that climate change has diverse regional and seasonal impacts on soil water availability across Europe. An increase in surface water availability has been reported for different warming levels for the Alpine and Boreal regions[2]. However, this increase is unevenly distributed over the year. Moreover, soil water availability seems to decrease significantly throughout Europe during seasons relevant for plant development (for example, summer and fall). Economic assessments of climate change adaptation for the agricultural sector are often based on temperature-related characteristic curves[17]. These analyses could benefit from incorporating soil moisture because it constitutes the primary source of water for plant growth.

The exacerbation of drought conditions in the Mediterranean under global warming of 1.5 K and 2 K will be unprecedented since the last millennium[22]. If a global warming of 3 K is reached, southern Spain and probably Italy and Greece will turn "into a desert"[29]. This unprecedented change will also have severe impacts on Mediterranean vegetation and biodiversity, and thus on ecosystems and their services. The strong reductions in soil water availability during dry periods are mostly related to decreases in precipitation and increases in evapotranspiration[2] (see Supplementary Figs. 3 and 4). The relatively large decreases in soil water availability noted in this region are related to the greater increases in the maximum

Table 1 | Multimodel ensemble median results for the area under drought, drought duration and months under drought conditions per year for different levels of global warming and stratified for the IPCC regions

Warming level	Atlantic	Continental	Boreal	Mediterranean	Alpine North	Alpine South
Drought area (% of total area)						
Reference	21.9	34.7	19.4	28.2	41.3	28.9
1.0 K	24.0	36.8	25.2	29.8	31.8	28.7
1.5 K	23.5	35.1	24.7	34.1	34.5	28.7
2.0 K	22.8	35.8	23.4	38.4	34.8	29.4
2.5 K	26.5	36.1	23.0	41.0	35.9	34.4
3.0 K	27.8	39.9	16.4	49.1	41.1	37.1
Drought duration (months)						
Reference	31.5	32.5	25.0	28.0	12.0	37.0
1.0 K	32.0	38.5	25.0	41.0	22.0	40.0
1.5 K	52.5	60.0	25.0	58.0	20.5	56.0
2.0 K	60.5	65.5	32.5	71.0	21.0	68.5
2.5 K	84.0	86.5	41.5	89.0	18.5	86.5
3.0 K	101.5	121.5	59.5	125.0	17.0	124.5
Drought months per year						
Reference	2.0	2.0	1.9	2.1	1.9	2.0
1.0 K	2.0	2.1	2.0	2.6	1.7	1.9
1.5 K	2.7	2.6	2.4	3.2	1.9	2.3
2.0 K	3.0	2.8	2.5	3.7	2.0	2.7
2.5 K	3.3	3.1	2.7	4.5	2.2	3.2
3.0 K	3.8	3.9	2.9	5.6	2.4	3.9

The period of 1971–2000 is used as a reference.

daytime temperatures compared to other regions[30]. Whether economic adaptation assessments[17] can properly assess such severe changes remains an open question. Note that while we estimate soil moisture for a 2-m-deep soil column, many plants, particularly crops, do not have roots that extend to that depth. Consequently, we probably underestimate the effects of soil moisture droughts in the top-soil layers because these layers tend to dry faster than the lower soil layers[8].

We relate our results to the 2003 drought event (estimated based on historical observations, see Methods) to illustrate the severity of the projected changes. In water-limited regimes, agricultural droughts are intrinsically related to significant reductions in evapotranspiration and gross primary production (GPP), as well as the occurrence of heat waves. For example, Europe emitted an amount of CO_2 that corresponds to the amount that is normally sequestrated in four years during the 2003 drought event[19]. In the future, drought events that are similar in magnitude and extent to that of 2003 will be twice as frequent. In detail, our results indicate that the increase in frequency, which is defined as the ratio of SMI under a warming of 3 K with respect to that of the reference period, is approximately 2.0 (±0.33). The estimated average soil water deficit during the 2003 drought event was 27.6 mm. The change in the drought threshold at a warming level of 3 K (Fig. 3) is of the same order of magnitude as the average deficit during the 2003 event in most of the regions. This result implies that much of this event will not be classified as a drought in the future, and the projected droughts will be associated with substantially less available soil water than the 2003 event.

We estimate that 42% (±22%) more people will be located within areas that will endure extreme droughts under a warming level of 3 K compared to a warming level of 1.5 K (170 million people versus 120 million people, respectively; Fig. 4). In contrast, 15% of the population (83 million people) was located in drought-affected areas during the 2003 event. At the peaks of the largest droughts, the population located within areas under drought increases from 336 to 400 million people (Fig. 4), and these numbers correspond to 61% and 73% of the European population, respectively. The increases in population within drought prone areas mostly occur in the Atlantic, Continental and Mediterranean region, because drought area is increasing the most in these regions (Table 1). Global warming may constitute a new human health threat[31] and extreme droughts, under particular situations, may trigger migration[32]. For these reasons, further studies should be conducted to investigate the potential effects of future extreme droughts on the European society and potential mitigation strategies that aim to reduce their negative effects.

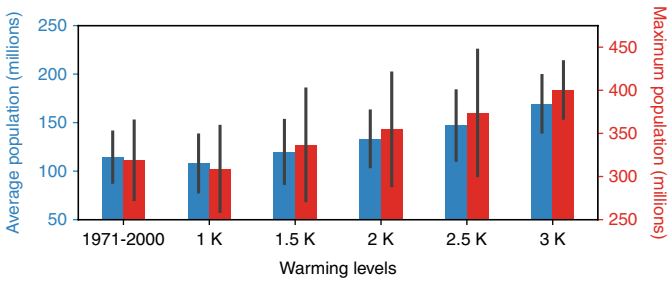

Fig. 4 | Changes in the European population within the largest drought events. The average (left *y* axis) and maximum (right *y* axis) European population located within the area enduring the largest drought at a given warming level (that is, those who will experience an alteration in standard living conditions during an event). Population data for 2005 are used for reference, and these data were obtained from the SEDAC dataset (http://sedac.ciesin.columbia.edu). Based on this dataset, the population of the study area is estimated to be approximately 550 million people. Error bars represent the ensemble s.d.

Overall, Europe will face unprecedented increases in the area affected by the largest soil moisture drought and the duration of such droughts if no adaptation is implemented during the coming decades (with respect to the historical period). The magnitudes of these increases depend strongly on the level of global warming. If future global temperatures will exceed 2 K above pre-industrial levels[11], our results show that drought areas will be up to 40% larger under a warming level of 3 K compared to a warming level of 1.5 K. Similarly, the drought duration will increase by three times between these two warming levels. Decreases in aridity are found only in the Alpine and Boreal regions during the winter and spring. Even if adaptation measures are successfully implemented, aridity will increase throughout the continent during the summer from less than 10 mm at a global warming of 1.5 K to approximately 20–35 mm at a global warming of 3 K. Such an increase in aridity is comparable to the deficit during the 2003 drought event. Our study therefore highlights the need to adapt to new normal conditions to minimize the impact of extreme drought events. The European agricultural sector must adapt to summers with reduced soil water, and the risk of land degradation and desertification in sensitive environments exists. Further research is urgently needed to assess the degree of impact of future extreme drought events on the European society as a whole, if increased aridity threatens minimum living conditions[32].

Methods

Methods, including statements of data availability and any associated accession codes and references, are available at https://doi.org/10.1038/s41558-018-0138-5.

Received: 23 November 2017; Accepted: 20 March 2018;
Published online: 23 April 2018

References

1. Dai, A., Trenberth, K. & Qian, T. A global dataset of Palmer Drought Severity Index for 1870–2002: Relationship with soil moisture and effects of surface warming. *J. Hydrometeorol.* **5**, 1117–1130 (2004).
2. Greve, P., Gudmundsson, L. & Seneviratne, S. I. Regional scaling of annual mean precipitation and water availability with global temperature change. *Earth Syst. Dynam.* **9**, 227–240 (2018).
3. Hirschi, M. et al. Observational evidence for soil-moisture impact on hot extremes in southeastern Europe. *Nat. Geosci.* **4**, 17–21 (2010).
4. Dai, A. Increasing drought under global warming in observations and models. *Nat. Clim. Change* **3**, 52–58 (2013).
5. Seneviratne, S. I. et al. Impact of soil moisture-climate feedbacks on CMIP5 projections: First results from the GLACE-CMIP5 experiment. *Geophys. Res. Lett.* **40**, 5212–5217 (2013).
6. Trenberth, K. E. et al. Global warming and changes in drought. *Nat. Clim. Change* **4**, 17–22 (2014).
7. Huang, J., Yu, H., Guan, X., Wang, G. & Guo, R. Accelerated dryland expansion underclimate change. *Nat. Clim. Change* **316**, 847–171 (2015).
8. Berg, A., Sheffield, J. & Milly, P. C. D. Divergent surface and total soil moisture projections under global warming. *Geophys. Res. Lett.* **44**, 236–244 (2017).
9. Cook, B. I., Ault, T. R. & Smerdon, J. E. Unprecedented 21st century drought risk in the American Southwest and Central Plains. *Sci. Adv.* **1**, e1400082–e1400082 (2015).
10. UNFCCC *Adoption of the Paris Agreement, Proposal by the President* Report No. FCCC/CP/2015/L.9 (United Nations, 2015).
11. Raftery, A. E., Zimmer, A., Frierson, D. M. W., Startz, R. & Liu, P. Less than 2°C warming by 2100 unlikely. *Nat. Clim. Change* **109**, 13915–13917 (2017).
12. Collins, M. et al. Quantifying future climate change. *Nat. Clim. Change* **2**, 403–409 (2012).
13. Prudhomme, C. et al. Hydrological droughts in the 21st century, hotspots and uncertainties from a global multimodel ensemble experiment. *Proc. Natl Acad. Sci. USA* **111**, 3262–3267 (2014).
14. Wanders, N., Wada, Y. & Van Lanen, H. A. J. Global hydrological droughts in the 21st century under a changing hydrological regime. *Earth Syst. Dynam.* **6**, 1–15 (2015).
15. James, R., Washington, R., Schleussner, C.-F., Rogelj, J. & Conway, D. Characterizing half-a-degree difference: a review of methods for identifying regional climate responses to global warming targets. *WIREs Clim. Change* **8**, 1–23 (2017).
16. Wilhite, D. *Drought: A Global Assessment* Vol., I. 3–18 (Routledge, London, 2000).
17. Moore, F. C. & Lobell, D. B. Adaptation potential of European agriculture in response to climate change. *Nat. Clim. Change* **4**, 610–614 (2014).
18. Van Lanen, H. A. et al. Hydrology needed to manage droughts: the 2015 European case. *Hydrol. Process.* **30**, 3097–3104 (2016).
19. Ciais, P. et al. Europe-wide reduction in primary productivity caused by the heat and drought in 2003. *Nature* **437**, 529–533 (2005).
20. Samaniego, L., Kumar, R. & Zink, M. Implications of parameter uncertainty on soil moisture drought analysis in Germany. *J. Hydrometeorol.* **14**, 47–68 (2013).
21. Samaniego, L. et al. Propagation of forcing and model uncertainties on to hydrological drought characteristics in a multi-model century-long experiment in large river basins. *Climatic Change* **141**, 435–449 (2016).
22. Lehner, F. et al. Projected drought risk in 1.5°C and 2°C warmer climates. *Geophys. Res. Lett.* **44**, 7419–7428 (2017).
23. Sheffield, J., Wood, E. F. & Roderick, M. L. Little change in global drought over the past 60 years. *Nature* **491**, 435–438 (2012).
24. Warszawski, L. et al. The Inter-Sectoral Impact Model Intercomparison Project (ISI–MIP): Project framework. *Proc. Natl Acad. Sci. USA* **111**, 3228–3232 (2014).
25. Samaniego, L. *EDgE Model Chain and Development of Sectoral Climate Impact Indicators* (Copernicus Climate Change Service, 2017); http://edge.climate.copernicus.eu
26. Kovats, R. et al. in *Climate Change 2014: Impacts, Adaptation and Vulnerability* (eds Barros, V. et al.) 1267–1326 (Cambridge Univ. Press, Cambridge, 2011).
27. Metzger, M. J., Bunce, R. G. H., Jongman, R. H. G., Mücher, C. A. & Watkins, J. W. A climatic stratification of the environment of Europe. *Glob. Ecol. Biogeogr.* **14**, 549–563 (2005).
28. Rötter, R. P., Carter, T. R., Olesen, J. E. & Porter, J. R. Crop–climate models need an overhaul. *Nat. Clim. Change* **1**, 175–177 (2011).
29. Guiot, J. & Cramer, W. Climate change: The 2015 Paris Agreement thresholds and Mediterranean basin ecosystems. *Science* **354**, 465–468 (2016).
30. Seneviratne, S. I., Donat, M. G., Pitman, A. J., Knutti, R. & Wilby, R. L. Allowable CO_2 emissions based on regional and impact-related climate targets. *Nature* **529**, 477–483 (2016).
31. Robine, J.-M.et al. Death toll exceeded 70,000 in Europe during the summer of 2003. *C. R. Biol.* **331,** 171–178 2008).
32. Wilbanks, T. et al. in *Climate Change 2007: Impacts, Adaptation and Vulnerability* (eds Parry, M. L. et al.) 357–390 (IPCC, Cambridge Univ. Press, 2007).

Acknowledgements

This study was partially performed under a contract for the Copernicus Climate Change Service (edge.climate.copernicus.eu). ECMWF implements this service and the Copernicus Atmosphere Monitoring Service on behalf of the European Commission. This study has been mainly funded within the scope of the HOKLIM project (www.ufz.de/hoklim) by the German Ministry for Education and Research (grant number 01LS1611A). We would like to thank P. Greve for providing data included in Supplementary Fig. 4. We acknowledge the funding from NWO Rubicon 825.15.003. We acknowledge the E-OBS dataset from the EU FP6 project ENSEMBLES (http://ensembles-eu.metoffice.com) and the data providers in the ECA&D project (http://www.ecad.eu). We would like to thank people from various organizations and projects for kindly providing us with the data that were used in this study, which includes ISI-MIP, JRC, NASA, GRDC, BGR and ISRIC. This study was carried out within the Helmholtz-Association climate initiative REKLIM (www.reklim.de).

Author contributions

L.S. and S.T. designed the study and wrote the manuscript. S.T., R.K., N.W. and M.P. conducted the model runs. O.R. and M.Z. conducted analysis of the data. All authors contributed to interpreting results.

Competing interests

The authors declare no competing interests.

Additional information

Supplementary information is available for this paper at https://doi.org/10.1038/s41558-018-0138-5.

Reprints and permissions information is available at www.nature.com/reprints.

Correspondence and requests for materials should be addressed to L.S.

Publisher's note: Springer Nature remains neutral with regard to jurisdictional claims in published maps and institutional affiliations.

Methods

Modelling chain. Daily temperature and precipitation values for the period 1950–2099 obtained from five CMIP5 GCMs (HadGEM2-ES, IPSL-CM5A-LR, MIROC-ESM-CHEM, GFDL-ESM2M and NorESM1-M) forced by three RCPs (RCP2.6, RCP6.0 and RCP8.5) are used as input to four HMs. These GCM data were made available by the ISI-MIP project[24] and are downscaled to a global resolution 0.5° and bias-corrected using a trend-preserving approach[33]. These models cover a range of 0.55 of the uncertainty of the entire CMIP5 ensemble for precipitation and 0.75 for temperature[34]. The uncertainty range of this five-member ensemble is comparable to that of a larger CMIP5 model ensemble (Supplementary Fig. 4)[2]. The 0.5° data are further disaggregated within the EDgE project[25] to a 5 km grid over Europe using the external drift kriging (EDK) approach. EDK constitutes the best linear unbiased estimator of the selected meteorological variable. This key characteristic of EDK constraints the mean of the interpolated (downscaled) values to not differ from the expectation of the meteorological variable at this location. Thus, EDK does not introduce artefacts (such as trends) into the original forcing. Another advantage of this approach is that it introduces orographic effects of precipitation and temperature that are not present in GCMs at coarser resolution, while maintaining the trend of the original data. The disadvantage of EDK is that it does not guarantee a conservation of mass and energy everywhere. Within the present study, however, the differences between the original and downscaled values are in general less than 1% (at most 5%) for precipitation and 0.1 K (at most 0.23 K) for temperature. These differences are smaller than the differences between the individual GCMs and the changes induced by climate change.

Two HMs (mHM and PCR-GLOBWB) and two land-surface models (Noah-MP and VIC) are used to simulate soil moisture up to a depth of 2 m. The same morphologic, land-cover and soil data are used to set up these models; thus, the differences among the model simulations are due solely to differences in the representations of processes used in the models. The mHM (www.ufz.de/mhm) is a process-based hydrologic model that was developed for use at scales ranging from 1 km to 50 km[35,36]. PCR-GLOBWB was developed to represent the terrestrial water cycle, including artificial water management, at global and continental scales, and it places special emphasis on the groundwater component[37]. Noah-MP is the land-surface component of the Weather Research and Forecast model, and it represents both the terrestrial water and energy cycles[38]. VIC was developed to provide a simplified representation of land-surface hydrological processes that would be suitable for implementation in a GCM[39]. The model parameters are calibrated using the E-OBS meteorological data[40] for nine distinct catchments located in Spain, the United Kingdom and Norway. An automatic calibration scheme is employed for mHM and PCR-GLOBWB[41]. Noah-MP is calibrated manually by adjusting the parameter describing surface evaporation resistance based on previous analyses[42]. The VIC parameters are taken from global simulation runs and are not calibrated using the E-OBS or observed river discharge datasets over the EU domain.

Drought frequencies related to changes of meteorological forcings. Supplementary Fig. 2 provides a comparison of the number of drought months for the individual hydrologic models, considering no adaptation to climate change for various levels of global warming. All hydrologic models show a similar increase in drought frequency in the Mediterranean region in southern Europe. This may be related to the relatively large decrease in annual precipitation of up to 25% at a warming level of 3 K (Supplementary Fig. 3). In central Europe, all models exhibit a smaller increase in drought frequencies in comparison to those in the Mediterranean, which could be expected given the smaller changes in projected precipitation (Supplementary Fig. 3). Projected temperature is increasing similarly in central Europe and the Mediterranean region, which highlights that the simulated evapotranspiration in this model ensemble is limited by water availability rather than by energy in this region. In contrast, precipitation is projected to increase in the Scandinavian region in northern Europe up to 20%. In this region, the hydrologic models differ in their projections of drought frequencies. For example, VIC and mHM show increases in this region, PCR-GLOBWB shows a mixed pattern and drought frequencies simulated by Noah-MP remain unchanged by global warming. Because all models are forced with the same meteorological data, the parameterization of snow processes in this cold region and the parameterization of ET have a strong impact on soil drought characteristics. For example, mHM allows ET when the surface is covered with snow, which is based on the model assumption that snow cover has a large subgrid variability. On the contrary, Noah-MP explicitly considers snow cover fractions within the calculation of evaporation. These results show that the HMs have relative larger differences over various regions. For this reason, we consider it fundamental to use a multimodel ensemble for climate change drought analysis.

Model verification. Streamflow simulations from the four hydrologic models, driven by five GCMs, were compared against observations during the historical 30-year period (1966–1995). Here, we analyse the model skill for reproducing the median daily flows (p50) over 357 gauging stations located across the EU domain (Supplementary Fig. 5). The gauges have been selected from the Global Runoff Data Centre database. All gauges have a complete 30-year period (1966–1995) of daily observations across the modelling domain, which allows for a robust statistical analysis. Additionally, these basins have an error of less than 10% in the basin delineation and the median basin area is 1,680 km^2. Overall, the ensemble model simulations show reasonably high skill in capturing the observed variability of p50, with a correlation coefficient value of 0.92 (Supplemetary Fig. 5e) and the mean relative bias is 35%. In general, the model combinations (GCM/HM) seem to slightly overestimate the observed p50 values, with mHM being closest to observations compared to the Noah-MP, PCR-GLOBWB and VIC model simulations. The basins in the central EU region and in the Iberian peninsula generally exhibit a positive bias (Supplementary Fig. 5f). We note that these verifications are quite rigorous as the hydrologic models are forced with GCM simulated datasets, rather than observed meteorological datasets. This implies that a comparison of simulated and observed streamflow for specific time points is not feasible because GCM-based simulations do not reproduce observed weather and thus events.

Estimation of warming levels. Within this study, the global warming levels for 1, 1.5, 2, 2.5 and 3 K are identified employing a time sampling approach[15]. The 30-year average temperature of 1971–2000 is used as a reference. The pre-industrial warming between the periods 1881–1910 and 1971–2000 is assumed to be 0.46 K[43]. This offset is subtracted from the warming levels for determining the 30-year periods for the specific global warming. These periods are identified as follows. For each GCM and RCP, the 30-year global average temperature for all 30-year periods between 1960 and 2099 is calculated (prepending the historical data to each RCP). The period when a 30-year global average temperature first reaches or exceeds a given global warming (1, 1.5, 2, 2.5, and 3 K minus 0.46 K offset) is then noted[15]. The procedure is illustrated in Supplementary Fig. 6 for all GCMs and RCPs. It is worth mentioning that other periods than 1881–1910 have been suggested to represent pre-industrial conditions, which might lead to offsets that are 0.11 K higher than the one used in this study[44]. We recalculated the periods based on this adjusted threshold and found shifts of 2 to 6 years (not shown). Given the fact that our analysis is using simulated soil moisture of 30-year periods, we expect little influence of the adjusted offset on our results.

In total, 15 GCM realizations reach 1 K, 14 reach 1.5 K, 13 reach 2 K and 8 reach 2.5 K and 3 K global warming. As four HMs are used in this study, the obtained sample sizes are sufficiently large to quantify extreme soil moisture droughts for each level of global warming.

SMI and drought characteristics. The SMI for a given cell and month is estimated as

$$\mathrm{SMI}_t = \widehat{F}_T(x_t) \tag{1}$$

and it represents the quantile at the soil moisture fraction value x (normalized against the saturated soil water content). x_t denotes the simulated monthly soil moisture fraction at a time t and $\widehat{F}_T$ is the empirical distribution function estimated using the kernel density estimator $\widehat{f}_T(x)$ of the corresponding calendar month at time t. $\widehat{f}_T(x)$ is estimated as

$$\widehat{f}_T(x) = \frac{1}{nh}\sum_{k=1}^{n} K\left(\frac{x-x_k}{h}\right) \tag{2}$$

Here, $x_1, \ldots, x_n$ represents the simulated soil moisture fraction of a given calendar month during the reference period T; n denotes the number of calendar months within a given period (that is, 30 for a 30-year period); and K represents a Gaussian kernel function with a bandwidth h. The bandwidth is estimated by minimizing a cross-validation error estimate[20] for the reference period separately for each calendar month, grid cell, LSM/HM and GCM combination to ensure comparability across time, space and model combinations. A cell at time t is under drought when $\mathrm{SMI}_t < \tau$. Here, τ denotes that the soil water content in this cell is less than the values occurring $\tau \times 100\%$ of the time. In this study, τ is set to 0.2. All drought events are identified using a multitemporal clustering algorithm[20]. This algorithm first masks all cells at each time step that fulfil $\mathrm{SMI} \leq \tau$ and consolidates adjacent cells to a drought event. Second, drought events at consecutive time steps that share a minimum overlapping area are consolidated into a single event. Third, drought statistics (such as areal extent, duration) are estimated for all identified drought events. The mean duration (D) of a drought event is then defined as the mean of the drought duration estimated over every cell affected by a drought event. This statistic is given in months. The mean areal extent (A) is defined as the average of the region under drought from the onset until the end of the drought event, which is then expressed as a percentage of the total surface area of the region. It should be noted that the value of the threshold τ determines A and D. Sensitivity analysis, however, shows that the rate of increase of these characteristics between two warming levels is invariant of the value of τ (compare Fig. 1 and Supplementary Fig. 1). The reference period T within the estimation of the $\widehat{F}_T$ is chosen in two ways to quantify the effect of adaptation to climate change: (1) T is chosen as 1971–2000 to calculate the drought area and duration for all warming levels, which represents no adaptation to climate change, (2) T is identical to the period when a global warming level has been reached, which represents adaptation to

climate change[14]. In the latter case, it depends on the amount of global warming, the GCM and the RCP considered.

Estimation of available soil water. The changes in the water soil storage (aridity) that occur at the different warming levels is estimated by varying the reference period from T_0 to T_Δ, where T_0 denotes the historical reference period (1971–2000), and T_Δ denotes the period until a particular value of ΔK is reached in a given RCP and GCM combination. Based on these two periods, the change in aridity within a region (as represented by the average over all of the cells within the region) for a given RCP-GCM-HM combination is estimated as

$$\delta x_\Delta = \langle \overline{\widehat{F}^{-1}_{T_\Delta}(\tau)} \rangle - \langle \overline{\widehat{F}^{-1}_{T_0}(\tau)} \rangle \quad (3)$$

The operator $\langle \cdot \rangle$ denotes the ensemble mean, and the overline indicates the spatial average. Finally, the seasonal averages are estimated from the values obtained for each month. This index is depicted in Fig. 3. Note that the threshold τ is kept constant (at 0.2) for T_0 and T_Δ. The absolute soil moisture thresholds (for example, $\widehat{F}^{-1}_{T_\Delta}(\tau)$), on the other hand, depend on the period.

Estimation of soil water deficit for the 2003 event. For a given drought event occurring in a period T, the soil water deficit in a given grid cell is estimated by

$$d_i{}^T(t) = [\widehat{F}^{-1}_{T,i}(\tau) - x_i(t)]_+ \quad (4)$$

The average deficit estimated over the lifespan of a drought event occurring in a period T is given as

$$d^T = \overline{\frac{1}{n_T} \sum_{t \in T} d_i{}^T(t)} \quad (5)$$

Here, n_T denotes the number of months under drought in the period T and the overbar indicates the spatial average. The operator $[\cdot]_+$ denotes the positive part function. The soil water deficit for the 2003 event is estimated as indicated above with every HM forced with the E-OBS[40] meteorological data (1950–2015). The period T corresponds to 1960–2002. The ensemble average is afterwards estimated to be 27.6 mm.

Comparison of SMI and PDSI. Numerous studies on drought research used the PDSI[1,6,23,45]. The PDSI is a water budget accounting index that cumulates soil moisture anomalies derived from monthly precipitation and temperature. Here, we use the self-calibrating version of PDSI[46] at the monthly timescale. PDSI requires two input parameters for every grid cell: the latitude of the considered location and the available water holding capacity (AWC). The latter is derived using the same soil dataset used for the hydrologic models and the multiscale parameter regionalization (MPR) method used in the mHM[35]. The calibration period for the PDSI is set to 1971 to 2000, which is consistent with the period for the estimation of the kernel density function of the SMI. Subsequently, both indices (SMI and PDSI) are evaluated during the period 2010 to 2099. We present results for one location in Eastern Germany (latitude: 51.09° N, longitude: 12.89 ° E) to discuss the differences between the PDSI and the SMI. However, the same features discussed below were also observed at locations in Southern France, Spain and England.

The RCP 2.6 scenario results in stationary SMI and PDSI data without any significant trend (Supplementary Fig. 7). This could be expected because the RCP 2.6 scenario leads to a projected increase in global mean temperature of 0.3–1.7 K until the end of the 21st century. All indices detect more droughts under RCP 6.0 (Supplementary Fig. 8) and RCP 8.5 (Supplementary Fig. 9) compared to RCP 2.6. However, there are substantial differences between the PDSI and SMI. Most importantly, the median PDSI indicates extreme drought conditions for the last third of the twenty-first century for both RCP 6.0 and RCP 8.5. In the latter case, the median PDSI shows a strong negative trend. For the same period, the median SMI indicates non-drought conditions for the majority of time points. This indicates that the PDSI is extremely sensitive to the projected climate change in this region. It is worth noting that climate change in this region is mostly increasing temperature, whereas annual precipitation increases by less than 10% (Supplementary Fig. 3). It is known that the PDSI method using the temperature-based Thornthwaite PET scheme is oversensitive to changes in temperature and that the Penman–Monteith method provides a less biased estimate[23]. The hydrologic models mHM and PCR-GLOBWB also use a temperature-based PET formulation (that is, the Hargreaves–Samani equation[47]), but show a similar behaviour to Noah-MP and VIC (Supplementary Figs. 7–9), which do not use a PET approach and calculate the full energy balance at the land surface.

These results highlight that the combination of a temperature-based PET approach with the conceptualization of the PDSI leads to an overestimation of drought conditions. On the contrary, a drought index derived from hydrologic models (that is, mHM and PCR-GLOBWB) that use a temperature-based PET scheme does not exhibit such behaviour. The reason for this difference stems from the way these indices are estimated. PDSI is an autoregressive model of the type

$$X_t = pX_{t-1} + qZ_t \quad (6)$$

that estimates the current PDSI value (X_t) based on the previous value of the index and the current soil moisture anomaly Z_t[46]. Here p and q are the so-called Palmer duration factors to be determined empirically for every location. Z_t is determined with a two-layer water balance model and several empirically parameters that "allow for accurate comparisons of PDSI values over time and space"[46]. The autoregressive conceptualization of PDSI under a non-stationary climate (that is, increasing temperature, PET and soil moisture anomalies under RCP6.0 and RCP8.5) induces a negative drift from the long-term mean. By contrast, SMI is by definition bounded between zero and one because it corresponds to the respective quantiles of the simulated soil moisture (see section above).

Population in drought areas. For each member of the multimodel ensemble, the spatio-temporal evolution of the largest drought event is identified during the reference period T_0 and all of the 30-year periods representing different levels of global warming T_Δ. This information is then overlaid with the population density to estimate the population located in the area under drought at a given point in time. Based on these results, we estimate the average and maximum populations affected over the lifespan of the drought. To identify the effect of future droughts, we use the distribution of the population of Europe in 2005. The UN-adjusted Gridded Population of the World, dataset, version 4, was obtained from SEDAC (http://sedac.ciesin.columbia.edu). The year 2005 is selected because it best represents the population distribution during the 2003 event, which is used in this study as a reference. According to this dataset, the population of the entire domain is approximately 550 million people. This analysis does not account for demographic changes.

Data availabilty. All information used in this study has been obtained from the following open sources: Terrain elevation EU-DEM and GOTOPO30 from https://lta.cr.usgs.gov/GTOPO30 and http://www.eea.europa.eu/data-and-maps/data/eu-dem; the river database CCM2 v2.1 from http://ccm.jrc.ec.europa.eu/php/index.php?action=view&id=23; Soils texture maps SoilGrids1km from http://www.isric.org/content/input-data-soilgrids; the land cover product GlobCOVER v2 from http://due.esrin.esa.int/page_globcover.php; the land-cover products CLC00, CLC06, CLC12 and CLC90 v18.4 from http://land.copernicus.eu/pan-european/corine-land-cover; the hydrogeology map IHME1500 v11 from http://www.bgr.bund.de/ihme1500; the CMIP5 climate projections from https://www.isimip.org/outputdata/isimip-data-on-the-esgf-server/; the historical forcings E-OBS v12 from www.ecad.eu/E-OBS/; and the GRDC streamflow data from http://www.bafg.de/GRDC. Finally, the EDgE simulations are available at http://edge.climate.copernicus.eu, and the data that support the findings of this study are available from the corresponding author upon request.

References

33. Hempel, S., Frieler, K., Warszawski, L., Schewe, J. & Piontek, F. A trend-preserving bias correction — the ISI-MIP approach. *Earth Syst. Dynam.* **4**, 219–236 (2013).
34. McSweeney, C. F. & Jones, R. G. How representative is the spread of climate projections from the 5 CMIP5 GCMs used in ISI-MIP? *Clim. Serv.* **1**, 24–29 (2016).
35. Samaniego, L., Kumar, R. & Attinger, S. Multiscale parameter regionalization of a grid-based hydrologic model at the mesoscale. *Water Resour. Res.* **46**, W05523 (2010).
36. Kumar, R., Samaniego, L. & Attinger, S. Implications of distributed hydrologic model parameterization on water fluxes at multiple scales and locations. *Water Resour. Res.* **49**, 360–379 (2013).
37. Sutanudjaja, E. H. et al. PCR-GLOBWB 2: a 5 arc-minute global hydrological and water resources model. *Geosci. Model Dev. Discuss.* **2017**, 1–41 (2017).
38. Niu, G.-Y. et al. The community Noah land surface model with multiparameterization options (Noah-MP): 1. Model description and evaluation with local-scale measurements. *J. Geophys. Res.* **116**, D12109 (2011).
39. Liang, X., Lettenmaier, D., Wood, E. & Burges, S. A simple hydrologically based model of land-surface water and energy fluxes for general-circulation models. *J. Geophys. Res. Atmos.* **99**, 14415–14428 (1994).
40. Haylock, M. R. et al. A European daily high-resolution gridded data set of surface temperature and precipitation for 1950–2006. *J. Geophys. Res.* **113**, D20119 (2008).
41. Rakovec, O. et al. Multiscale and multivariate evaluation of water fluxes and states over European river basins. *J. Hydrometeorol.* **17**, 287–307 (2016).
42. Cuntz, M. et al. The impact of standard and hard-coded parameters on the hydrologic fluxes in the Noah-MP land surface model. *J. Geophys. Res. Atmos.* **121**, 10676–10700 (2016).
43. Vautard, R. et al. The European climate under a 2 degrees C global warming. *Environ. Res. Lett.* **9**, 034006 (2014).

44. Hawkins, E. et al. Estimating changes in global temperature since the preindustrial period. *Bull. Am. Meteorol. Soc.* **98**, 1841–1856 (2017).
45. Palmer, W. C. *Meteorological Drought* Research Paper 45 (Office of Climatology, Weather Bureau, 1965).
46. Wells, N., Goddard, S. & Hayes, M. J. A self-calibrating Palmer Drought Severity Index. *J. Clim.* **17**, 2335–2351 (2004).
47. Hargreaves, G. H. & Samani, Z. A. Reference crop evapotranspiration from temperature. *Appl. Eng. Agric.* **1**, 96–99 (1985).